Nanoscale Advances



MINIREVIEW

View Article Online
View Journal | View Issue



Cite this: *Nanoscale Adv.*, 2019, **1**, 1672

# Self-assembled colloidal arrays for structural color

Panmiao Liu,[a] Ling Bai,[c] Jianjun Yang,[a] Hongcheng Gu,[b] Qifeng Zhong,[d] Zhuoying Xie *[c] and Zhongze Gu*[bc]

Received 5th November 2018
Accepted 25th February 2019

DOI: 10.1039/c8na00328a

rsc.li/nanoscale-advances

Structural color materials that are colloidally assembled as inspired by nature are attracting increased interest in a wide range of research fields. The assembly of colloidal particles provides a facile and cost-effective strategy for fabricating three-dimensional structural color materials. In this review, the generation mechanisms of structural colors from colloidally assembled photonic crystalline structures (PCSs) and photonic amorphous structures (PASs) are first presented, followed by the state-of-the-art and detailed technologies for their fabrication. The variable optical properties of PASs and PCSs are then discussed, focusing on their spatial long- and short-order structures and surface topography, followed by a detailed description of the modulation of structural color by refractive index and lattice distance. Finally, the current applications of structural color materials colloidally assembled in various fields including biomaterials, microfluidic chips, sensors, displays, and anticounterfeiting are reviewed, together with future applications and tasks to be accomplished.

## 1. Introduction

Natural colors, as widely displayed by animals, plants, and other organisms, are mainly generated by pigments, structural colors, fluorescence, or their combinations.[1–7] Unlike pigment and fluorescence, a structural color is generated from light reflection, diffuse reflection, diffraction, and interference with spatially ordered nano- or microstructures in organisms.[8] Over the past 515 million years, organisms in nature have been using these nano- or microstructures to produce structural colors to embellish their appearances. Modern studies involving structural colors date back to 1665, when Hooke first proposed that the color of silverfish came from microstructures. In 1730, Newton explained the principle of structural color generation in peacock feathers. A detailed explanation of the structural colors was completed by Anderson and Richards in 1942, which was accomplished by the application of nanoscopic methods such as electron microscopy.[9] Biophotonic crystals were first reported by Parker in 2001.[10] Since

[a]*Department of Anesthesiology, The First Affiliated Hospital of Zhengzhou University, Zhengzhou, 450052, China*

[b]*Key Laboratory of Child Development and Learning Science, Research Center for Learning Science, Southeast University, Nanjing, 210096, China. E-mail: gu@seu.edu.cn*

[c]*State Key Laboratory of Bioelectronics, School of Biological Science and Medical Engineering, Southeast University, Nanjing, 210096, China. E-mail: zyxie@seu.edu.cn*

[d]*Department of Pharmaceutical Equipment and Electronic Instruments, School of Engineering, China Pharmaceutical University, 24 Tongjia Lane, Gulou District, Nanjing 210009, China*

*Panmiao Liu received her M.Sc. degree from Chemical Engineering at the Southeast University in 2014. She received her Ph.D. degree in Biomedical Engineering at the Southeast University in 2018. Now she works as a postdoctor in Department of Anesthesiology of the first affiliated hospital of Zhengzhou University. Her current research interests are synthesis of nanoparticles and biomaterials, self-assembly of nanomaterials and structurally colored materials.*

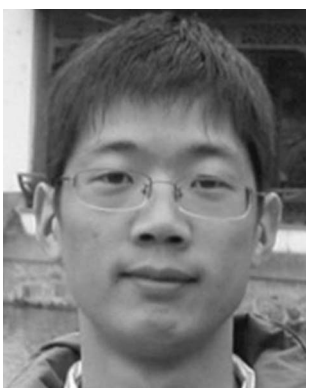

*Zhuoying Xie is currently an associate professor at the State Key Laboratory of Bioelectronics. He received his Bachelors degree in Biomedical Engineering at the Southeast University in 2005 and PhD degree in 2011. In 2009–2010, he worked as a research scholar in Prof. Geoffrey A. Ozin's group in University of Toronto. His current scientific interests are focused on self-assembly of nanomaterials, PCSs and biosensors.*

then, research into biostructural color nanomaterials has rapidly developed. These studies have shown that rich colors in bird feathers and butterfly wings were mainly caused by the interference of light. For example, the blue color of the head and neck skin of turkeys and the blue color of facial, hips, and reproductive area of primates are both derived from light scattering by a large number of fine particles in the corresponding epidermal tissues. In addition, organisms with a dynamic structural color were found to be able to control their colors and patterns to transmit information about sexual desire, warnings, and camouflage.[11] These changing colors can be directly applied to the construction of tunable optical devices. The modulation of color at the subcellular level also provides a good prototype for the development of tunable color display devices.

In the recent decades, scientists have devoted considerable effort to mimic the fantastic photonic materials present in natural biostructures. However, these structures are usually very subtle and complex, which are difficult to mimic using the widely popular top-down technologies, such as lithography. Alternatively, the self-assembly of colloidal particles as a facile and cost-effective bottom-up strategy for the fabrication of photonic materials has been rapidly developing in the last two decades, which has led to a wider range of applications. In the following sections, a detailed introduction on the color mechanism and colloidal assembly approaches for photonic crystalline structures (PCSs) and photonic amorphous structures (PASs) has been presented. The angle independence and optical modulation of PCSs and PASs are separately discussed. The important applications of these structural color materials are presented thereafter, followed by some perspectives on their future development and challenges toward their practical applications.

## 2. Mechanism for generation of structural color by colloidal assembly

Yablonovitch and John first proposed PCSs in 1987.[12,13] The periodic dielectric structures of PCSs were proven to generate a photonic bandgap (PBG) from the perspective of the electromagnetic field. Light with a certain wavelength in the PBG is forbidden to propagate. A structural color is generated when the PBG of a PCS is in the visible region (Fig. 1a). The characteristic wavelengths of the diffracted light can be expressed by the following Bragg's equation:[14,15]

$$m\lambda = 2nd \sin \theta$$

where $m$ is the series of diffraction, $\lambda$ is the wavelength of diffraction, $n$ is the average refractive index (RI), $d$ is the lattice constant, and $\theta$ is the angle between the incident light and normal crystal plane. According to the theoretical basis provided by the above formula, any change in the parameters of the Bragg equation could be used in principle to design and prepare a modulated structural color material. For example, the structural colors of PCSs change with the viewing or incident light angle.[16]

From the colloidal point of view, it is a real challenge to fabricate PASs with both perfect crystal and perfectly disordered structure. As compared to PCSs, PASs have degraded arrangements of subunits, and therefore, they exhibit unsaturated structural colors. These subunits could be colloidal particles, air cavities, and fiber structures with submicron feature sizes, and they could be widely found in many living objects.[17–23] It is believed that the lack of a long-range order in PASs suppresses the interferences of light and increases the scattering effect (Fig. 1b). Among the scattering effects, the Mie resonances of single particles with high refractive indexes in the region of a few hundred nanometers could also generate color.[24,25] A hypothesis from Dr Miyazaki and co-workers[26] suggested that PASs could form a similar PBG with PCSs, and both coherent interference of scattered waves from periodic structure and Mie resonances of bonding/antibonding states within each particle could contribute toward the PBG. When the scattering effect is not dominant, the main scattering peak ($\lambda_{max}$) of PASs (0-order) could be estimated using Bragg–Snell law:

$$\lambda_{max} = 2d(n_{eff}^2 - \sin^2 \alpha)^{1/2}$$

where $d$ is the (111) plane interplanar spacing, $n_{eff}$ is the effective refractive index, and $\alpha$ is the angle of incidence.

*Zhongze Gu graduated from Southeast University in 1989 and got his M.S. in 1992 there. He went to the University of Tokyo in 1994 and obtained his Ph.D. in 1998. Since then, he had been working as a researcher at the Kanagawa Academy of Science and Technology. Since 2003, he began to work at Southeast University as a professor Cheung Kong Scholars of Biomedical Science and Medical Engineering. Now he is the dean of School of Biological Science and Medical Engineering, the director of State Key Laboratory of Bioelectronics. His researches related to bio-inspired intelligent materials, photonic colloidal crystal, biosensor and bioelectronics.*

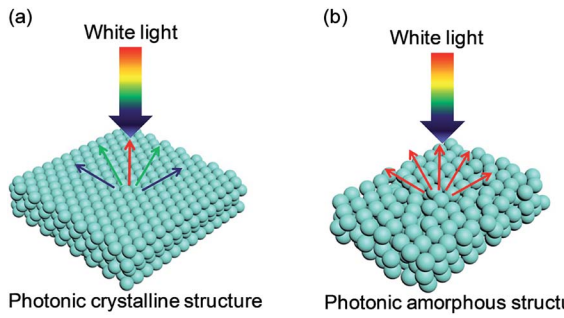


Fig. 1 Typical photonic nanostructures of colloidal assembled structural color: (a) highly ordered PCSs generating iridescence; (b) short-ordered PASs exhibiting non-iridescence.

Therefore, the structures present a low-angle-dependent structural color, which favor the applications of displays and sensors using structurally colored materials.[27–32]

## 3. Fabrication for structural color by colloidal assembly

Bottom-up colloidal assembly approaches are easy and cost-effective for the scalable production of structural color materials. In this section, we review the traditional and state-of-the-art self-assembly technologies for the fabrication of three-dimensional (3D) structural colors using colloidal materials with controllable long- and short-range orders.

### 3.1 Crystalline colloidal arrays

Methods based on the self-assembly of colloidal particles provide an elegant and efficient route for the generation of crystalline colloidal arrays. The first report involving the application of crystalline colloidal arrays to PCSs was reported by V. N. Bogomolov *et al.*,[33,34] followed by R. Mayoral *et al.*[35] Early research regarding colloidal assembly with periodic hexagonal arrays was inspired from the evaporating solutions of polymers under a flow of moist gas.[36] Xia *et al.* used a similar gas-flow force approach to assemble polystyrene (PS) particles into 3D crystalline colloidal arrays.[37] Although the proposed procedure is simple and practical, the device fabrication necessitates conventional photolithography. However, colloidal assembly technology is different from conventional photolithography; therefore, new technologies have emerged. Subsequently, evaporation-induced colloidal assembly is the most widely used method for constructing structural colors with crystalline colloidal arrays. One typical example is the vertical deposition method, which uses the solvent-evaporation-assisted method to assemble PCSs under the interaction of capillary force and surface tension. This method is also called the continuous convection self-assembly method and was first proposed by Nagayama *et al.*[38] When the substrate is vertically inserted into a colloidal solution, colloidal particles can self-assemble into PCSs on the substrate under the interaction of a capillary force and surface tension. Using this method, Colvin *et al.*[39] have successfully assembled large-area, highly ordered porous structural color materials.

Based on the vertical deposition method, a monolayer and even hundreds of layers of ordered colloidal crystals can be prepared on a vertically placed substrate by adjusting the temperature, humidity, concentration of colloidal solution, and growth time. However, because the colloidal particles deposited on the substrate induce low occupancy toward the total particles in the solution, the evaporation of the solvent results in a change in the concentration of the solution, which changes the thickness of the colloidal crystal along the growth direction. For colloidal particles with a larger particle size (>500 nm) and larger density, such as $SiO_2$, the sedimentation rate of the particles is larger than the evaporation rate of the solvent, and hence, colloidal crystals with large areas cannot be obtained. To resolve the problem of sedimentation of large particles, the methods of agitation, convection compensation, pulling, and flow control are proposed. For the agitation method, Ozin[40] formulated the assisted directed evaporation-induced self-assembly to avoid the sedimentation of large particles. A magnetic stirrer at a stirring speed of 100–300 rpm was placed at the bottom of the solution to avoid large particle precipitation in the process of solvent evaporation. For the convection compensation method, Norris[41] utilized the temperature gradient at the top and bottom of the container to produce continuous convection in the colloidal particles solution, thereby reducing the effect of sedimentation of large particles and yielding a colloidal crystal film assembled by $SiO_2$ particles (diameter: 855 mm) that had far fewer colloidal crystal defects than those observed in gravity sedimentation. Moreover, the single crystal range could reach the millimeter scale, which was 10–100 times larger than that obtained in the gravity sedimentation method. Gu[42] proposed a pulling approach instead of colloidal assembly that relies solely on the solvent evaporation method. The substrate was cleaned and clipped on the sample table and then vertically immersed in the colloidal solution at a certain concentration. The substrate was slowly pulled from the colloidal solution with sample stage upgrades by a computer-driven motor. Meanwhile, the colloidal particles effectively self-assembled into PCS films in the three-phase interface. The thickness of the colloidal crystal film can be controlled by a combination of the volume fraction of colloidal particles in the solution and the pulling speed of the motor. Unlike the vertical deposition method, the dipping approach could yield a higher-quality colloidal crystal film with a large area of uniform thickness. As the substrate growth rate is far greater than the evaporation rate of the solvent and the sedimentation rate of particles, this method can avoid the influence of colloidal particle concentration during solvent evaporation.

Field-induced self-assembly is also an effective approach for assembling monodisperse colloidal particles that form PCSs. Woodcock[43] prepared PCSs by gravity deposition and also made detailed theoretical calculations of the colloidal assembly. However, colloidal particles that are too big or too small are difficult to assemble into an ordered colloidal crystal structure by gravity sedimentation. Hence, C. López[44] proposed using the electrical properties of colloidal particles under an induced electric field to assemble the colloidal crystal. Based on the induced electric field method, Gu *et al.* developed an electrophoresis method to prepare thick PCS films by the capillary electrophoresis effect.[45] The particles were assembled into the PCS between the gaps by capillary force. The thickness of the film was tunable by controlling the evaporation of liquid from the capillary cell using the electrophoresis effect. In addition to opal PCSs, Gu *et al.* further developed a preparation strategy for the inverse opal PCS color films using the electrophoresis effect.[46] Because of external electric field forces, $SiO_2$ and $TiO_2$ can fill the voids of the opal templates constructed by vertical deposition (Fig. 2a). Inverse opal PCSs were obtained by removing the PS particles and sintering the oxide nanoparticles. The electrophoresis technique could be suitable for all the charged materials from which nanoparticles can be fabricated for the structural color of PCSs.

 

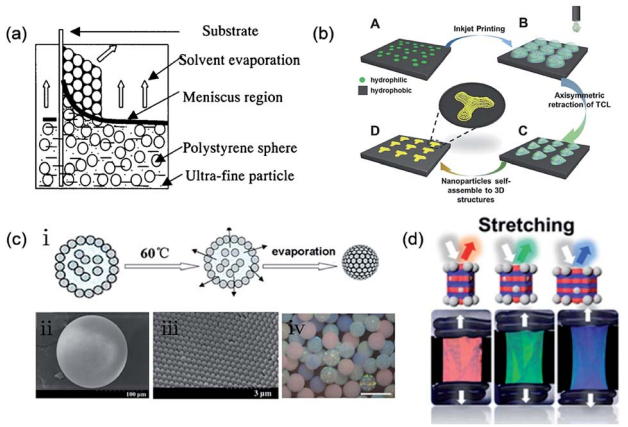


Fig. 2 (a) Schematic of the simple method of co-assembly by using the general vertical deposition method. Reproduced with permission.[46] Copyright 2001, American Chemical Society. (b) 3D PCSs induced by the asymmetric dewetting on hydrophilic–hydrophobic patterned substrate. Reproduced with permission.[53] Copyright 2015, Wiley-VCH. (c) (i) Process of particle assembly into a microsphere.[56] Copyright 2008, American Chemical Society. (ii) SEM image of the microsphere.[56] (iii) Particle arrangement on the surface of the microspheres.[50] Copyright 2006, Wiley-VCH. (iv) Image showing the different structural colored microspheres. Reproduced with permission.[57] Copyright 2009, Wiley-VCH. (d) Photonic films containing a non-close-packed face-centered-cubic array of silica particles embedded in an elastomer, where the inelastic particles enable elastic deformation and reversible color change, as observed in chameleons. Reproduced with permission.[69] Copyright 2017, American Chemical Society.

Spin coating is also a rapid and repeatable assembly method for preparing PCSs using solvent evaporation. In the spin-coating process, the solvent flows through the substrate at a high shear rate, which results in close packing of the colloidal particles on the substrate. An ordered PCS could be obtained by properly controlling the spin condition. Wu *et al.*[47] built an experimental system to assemble PS particles of a size ranging from 223 to 1300 nm and form a close-packed colloidal crystal using spin coating. Their detailed results provided a very valuable reference point for the efficient and controllable fabrication of large-scale and uniform PCS films with PS nanospheres of various diameters by spin coating. However, methods based on the evaporation of solvents are always accompanied by an increase in the volume fraction of the dispersed particles. The high particle concentration usually induces several cracks every 50–250 mm in solid colloidal crystal films, which has a strong effect on the structural color. As an improved approach, Gu *et al.*[48] explored the self-assembly of particles at the air–water–air interface to fabricate free-standing colloidal crystal films. This strategy enabled the creation of structural color films that were crack-free over several square millimeters. Furthermore, the air–water–air interface could provide a platform to control the dynamics of the colloidal self-assembly, which may have immense promise in photonic applications.

Apart from simple solvent evaporation methods, template-assisted colloidal assembly with a complex form also holds promising potential for applications in microphotonic crystal devices and chips. The controllable modification of the substrate surface enables the selective sedimentation of colloidal particles on the substrate surface.[49] Braun *et al.*[50] directly deposited colloidal particles onto a lithographically patterned Si substrate to prepare patterned crystalline colloidal arrays. Ozin *et al.*[51] used a patterned PDMS elastomeric stamp to create surface-confined patterned templates. Through a directed evaporation-induced self-assembly approach, planarized PCSs with controllable shape, size, and orientation could be fabricated. Although these methods can be used to efficiently prepare patterned PCSs, the fabrication of their assisted templates always relies on complicated lithography processes. As an improvement, Gu *et al.*[52] used a silane-modified $TiO_2$ film with patterned ultraviolet (UV) irradiation to obtain a two-dimensional (2D) hydrophilic- or hydrophobic-templated substrate. The colloidal crystals were selectively deposited in the hydrophilic region, subsequently forming patterned colloidal crystals by the pulling method. Further study showed that colloidal particles could be selectively deposited and composite PCS patterns could be obtained by repeating these steps. The greatest merit of this method is that it uses 2D-patterned substrates to achieve highly ordered 3D colloidal crystals and overcomes the weakness of the disordered arrangement of colloidal particles, which is often present in some chemical template methods. To achieve more precise control over the colored patterns, Song *et al.*[53] constructed controllable 3D structures and morphologies from a single droplet by inkjet printing. During solvent evaporation, the three-phase contact line of a single droplet containing colloidal particles tends to pin on the hydrophilic points and asymmetrically dewets the hydrophobic region, which results in lines, quadrilaterals, stars, hexagons, and octagons. The strategy of the patterned substrate inducing colloidal PCS patterning can be used to fabricate highly ordered structures; therefore, it can exhibit bright structural colors (Fig. 2b). In addition to the 2D-patterned substrate, a droplet containing several monodisperse colloidal particles could be used as a 3D template for forming spherical PCSs after the volatilization of the solvent. Yang *et al.*[54,55] used microfluidic technologies combined with the droplet template method to prepare monodisperse colloidal crystal microspheres. The size of the colloidal crystal microspheres can be effectively adjusted by the flow rate and concentration of the colloid solution. However, the stability of the microspheres assembled by the colloidal particles packing is weak, which hinders their real applications. To resolve the fragmentation of PCS spheres, Gu *et al.*[56–58] constructed $SiO_2$ PCS microspheres with high mechanical strength by sintering at a high temperature (Fig. 2c(i)). This high temperature could enhance the bonding between the colloidal particles, yielding a more stable microsphere. The surface of the microspheres obtained by this method was smooth and the colloidal particles inside the sphere were arranged in a standard hexagonal-packed structure (Fig. 2c(ii) and (iii)).

Colloidal particles could also self-assemble into non-close-packed PCSs (NCPPs).[59–63] Meseguer *et al.* found that NCPP exhibited better optical properties than their close-packed counterparts.[64] They also argued that NCPPs could be

fabricated by using a combination of colloidal self-assembly, thermal sintering, and etching techniques. In addition to solid-state NCPPs, colloidal particles could also form liquid-state NCPPs in a liquid medium. When high-charge-density colloidal particles in the dispersion medium reach a certain volume fraction, the colloidal particles can self-assemble into a 3D-ordered periodic structure because of the minimized electrostatic repulsion between the electric double layers on the surface of the colloidal particles.[65–67] Moreover, as the high volume fraction can compress the electric double layer, the crystal lattice and structural color of the colloidal crystals can be obtained by changing the particle concentration. However, because of the low elastic modulus, the crystal structure is easily damaged by forces such as weak shear, gravity, electric fields, and thermal shock from the surrounding materials, which results in an unstable system. To overcome this, researchers introduced a hydrogel monomer into the dispersion medium to lock into the crosslinked network-like solid hydrogel by photopolymerization.[68] Using this approach, Kim *et al.*[69] recently locked $SiO_2$ colloidal particles into an elastomer forming an NCPP array. Unlike the hydrogel film, PCS elastomer films could serve as an artificial skin for wide applications (Fig. 2d).

### 3.2 Amorphous colloidal arrays

Unlike PCSs, the fabrication of PASs needs control of the colloidal arrays in a disordered state. Like PCSs, PASs could also be assembled by uniform particles by means of an appropriate approach. Takeoka and Kazuhide *et al.*[70–72] constructed amorphous colloidal gels in suspension by assembling uniform colloidal particles. These studies showed that colloidal particles with lower particle concentrations were colorless in the suspension without any aggregation or sedimentation. However, above a certain particle concentration, the suspensions solidified and exhibited different structural colors depending on the particle concentrations (D, E, and F bottles in the lower panel of Fig. 3a). Further studies proved that the liquid–solid transition of the amorphous colloidal arrays was essentially caused by a colloidal glass transition. Another approach for PAS fabrication is to assemble cohesive core–shell colloidal particles.[73] According to the softness of the shells, the core–shell particles could easily assemble PASs through centrifugation. After packing, these particles exhibited angle-independent structural colors that could be tuned by changing the shell thickness, size of the core particle, or concentration of the particle suspension (Fig. 3b). The rapid dewetting approach is another effective colloidal assembly method for uniform particles to fabricate large-scale 3D PASs. Because of the rapid or nonequilibrium removal of the solvent by evaporation or infiltration, the colloids could hardly restore their equilibrium state through thermodynamic energy; therefore, their colloidal crystallization is considerably suppressed. The spray-coating method is a typical rapid dewetting method to fabricate 3D PASs (see schematic in Fig. 3c). A suspension of fine, submicron spherical particles was quickly sprayed onto the substrate surfaces. Because of the rapid evaporative effect of the solvent, the colloidal particles were dried in air and coated onto the glass plate to form a thin membrane in a powdered state.[74] In

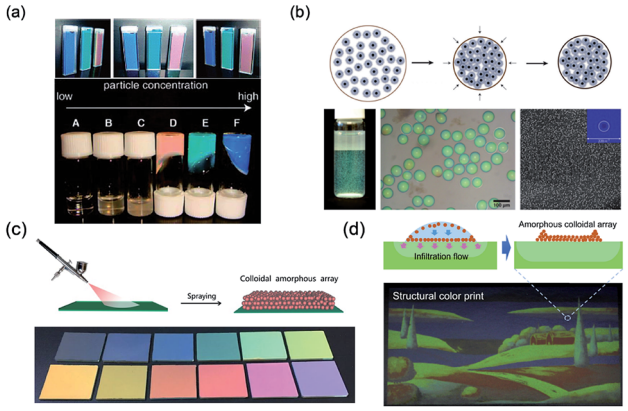


Fig. 3 (a) Pictures of gel particle suspensions. The suspensions have different viscosities and colors depending on the particle concentration. Reproduced with permission.[70] Copyright 2009, American Chemical Society. (b) Schematic of assembling soft cohesive particles into colored microspheres, and the photographs and SEM images of the obtained colored microspheres. Reproduced with permission.[73] Copyright 2014, Wiley-VCH. (c) Schematic of the spraying method used for amorphous structural color and different colors obtained that are tuned by the particle size. Reproduced with permission.[74] Copyright 2017, Royal Society of Chemistry. (d) Schematic of assembling oppositely charged particles in a layer-by-layer manner and the obtained colored films. Reproduced with permission.[75] Copyright 2018, John Wiley and Sons.

addition, infiltration-driven colloidal assembly is another newly developed rapid dewetting method for the large-scale fabrication of 3D PASs. When colloidal inks were printed onto liquid-permeable and particle-excluding substrates such as paper or anodic aluminum oxide (AAO) membranes, the rapid infiltration in the AAO membrane causes a downward microflow in the colloidal dispersion, which transports the particles downward and subsequently fixes them onto the substrates. Because the particles in a certain volume of liquid removed by infiltration are immediately fixed on the substrates, the concentration of particles in the remaining suspension remains nearly unchanged, which is too low for colloidal crystallization; therefore, PASs are finally formed (Fig. 3d).[75] Takeoka *et al.* used a layer-by-layer approach to assemble fine uniform colloidal particles forming PAS angle-independent structural color materials on the surface of a black plate. A large area of uniform PAS membranes was obtained by depositing alternating layers of charged colloidal particles and layers of an oppositely charged polyelectrolyte.[76]

By using nonuniform particles for the colloidal assembly, the tendency for colloidal crystallization during the self-assembly process could be considerably suppressed, which favors the formation of 3D PASs. In this regard, Lai *et al.*[77] dispersed nonuniform $SiO_2$ particles constructing a photocurable PAS resin in the resin prepolymer. They prepared composite resin films with high transparency and a uniform reflection-induced structural color through solidification by UV photopolymerization. The drying of biodisperse colloidal suspensions is also an effective method for fabricating structural PAS colors. The color of the obtained amorphous arrays depends on the weight ratio of the two differently sized PS particles.[78]

# 4. Angle dependence for structural color

## 4.1 Ordering of particles in colloidal arrays

Crystalline colloidal arrays with a long-ordered structure exhibit a bright structural color because of the narrow PBG. The color changes with the light incident/viewing angle, resulting in brilliant iridescent structural colors due to Bragg's diffraction. However, the angle dependence of such structural color hinders the construction of wide-viewing-angle optical materials and devices. In contrast, PASs with a short-range order yield a broader PBG through coherent reflection, which weakens the Bragg's diffraction effect. Therefore, PASs exhibit an angle-independent color. In other words, the structural color could be controlled by the degree of order of the colloidal particles. When the colloidal particles are ordered/assembled (PCSs), the present structural color changes with the angle of incident light. When the colloidal particles are short-ordered assembled (PASs), the structural color is independent of the angle.

## 4.2 Microscopic surface topography

An angle-independent structural color could also be obtained by the design of the microscopic surface topography of PCSs. Gu *et al.*[79] found that substrate wettability could be controlled by the self-assembly of particles on solid substrates. Both hydrophilic and hydrophobic substrates could be used to control the surface topography of colloidal crystals, separately leading to ring- and crater-shaped colloidal crystals (Fig. 4a). Song[80] and Gu *et al.*[81] further determined that the contact angle of the printed substrate on the optical properties of inkjet-printed colloidal PCS hemispheres was larger than 0.375: the colloidal PCS structural color was angle-independent (Fig. 4b). They further used angle-controlled color that was assembled into a color pattern design by means of inkjet printing (Fig. 4c). Inspired by the hemispherical shape of the angle-independent color, Gu's group[82] further developed novel PCS-colored materials with the desired feature of either anisotropic angle independence or full angle independence by using colloidal crystal fibers (CCFs) or colloidal crystal beads (CCBs) as their elements. They found that the films comprising CCFs could show anisotropic angle independence because of the circular symmetry of the CCF elements in their cross-section. These CCBs were composed of spherical colloidal crystal arrays with spherical symmetry, and they exhibited identical photonic responses independent of the rotation of the axes. Therefore, the PCS films composed of CCBs exhibited bright angle-independent structural colors (Fig. 4d). Such bright angle-independent colored films have promising potential applications in colored or information displays.

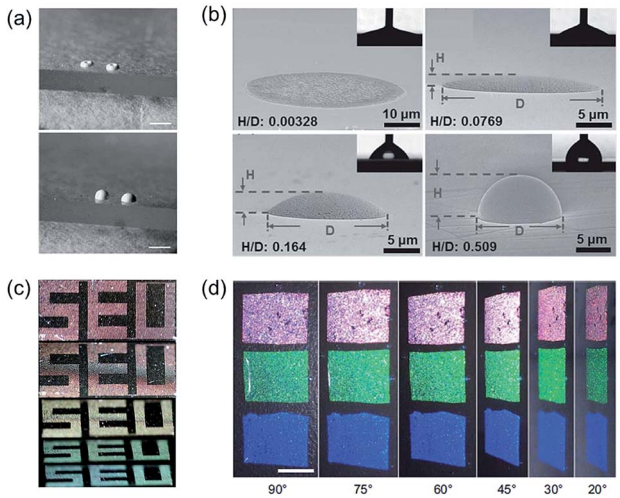


Fig. 4 (a) Schematic depiction of the aggregation of monodisperse spheres on hydrophilic and hydrophobic substrates. Reproduced with permission.[79] Copyright 2004, Springer Nature. (b) Side-view SEM images of the printed dots and domes on substrates with different $\theta_R$ values of 18.0° ± 5.7°, 39.3° ± 4.9°, 67.2° ± 3.6°, and 93.3° ± 1.9°. The *H*/*D* ratio is elevated with an increasing $\theta_R$. Reproduced with permission.[80] Copyright 2013, Wiley-VCH. (c) Three angle-controlled colors assembled by silica particles into the color pattern design by electrohydrodynamic jet printing. Reproduced with permission.[81] Copyright 2017, American Chemical Society. (d) Three angle-independent structural colored colloidal crystal beads composed of PCS films viewed at different angles. Reproduced with permission.[82] Copyright 2013, Wiley-VCH.

# 5. Tunable structural color

## 5.1 Modulation of RI

The structural color could be modulated by changing the difference in RIs between the building blocks and medium phase. The common building blocks of structural color materials using colloidal assembly are polymeric and silica materials with an intrinsically low RI (less than 1.6), which limits the possibility of forming a wider (even complete) PBG and exhibiting higher reflectivity. This results in low color visibility, which truly limits the potential applications of structural color materials. To overcome this problem, colloidal particles with high RI are developed. Inorganic colloidal particles, such as CdS, ZnS, and $TiO_2$, are synthesized to create structural color materials.[83–85] The intrinsically high RI of inorganic colloidal particles could improve the possibility of color visibility by self-assembling into a structural color, but obtaining larger quantities of monodisperse inorganic colloidal particles is still a major challenge because of the limitation of kinetics control during synthesis. The latter seriously limits the development of inorganic colloidal arrays in the structural color field.

Polymeric colloidal particles with high RI are also created. For example, Kawamura *et al.*[86] developed core–shell particles with melanin-like polydopamine (PDA) shell layers to fabricate structural color materials. Because of the high RI (~1.7–1.8) and light absorption of PDA layers, the assembled arrays exhibited highly visible structural color. However, the core–shell colloidal particles always need colloidal particles and additives, which adds complexity and difficulty to the construction process. Xiao *et al.*[87] proposed an easy method to directly achieve monodisperse PDA particles and also construct a highly visible structural color. Recently, Tang *et al.*[88] also created monodisperse polysulfide particles with an intrinsically high RI (as

high as 1.858) to construct structural color. The assembled arrays exhibited a highly visible color (Fig. 5a).

In addition to increasing the RI of the assembled colloidal particles, changing the RI of the medium phase could also adjust the structural color. The change is usually implemented by introducing new substances, such as selective absorption or penetration of solvents or gas molecules, high-temperature phase transition, photoinduced chromophore phase transformation, electric induction, and shape-induced liquid crystal molecular orientation. Gu *et al.*[89] placed photochromic dyes into silica PCS arrays and modified the structure from a spiropyran form to J-aggregates under UV light. This change effectively modulated the structural color of the PCSs. In addition, based on the changing of RI, Ge *et al.*[90] recently developed a photonic crystal gel sensor to monitor homologues, isomers, and solvents with similar structures and physical properties. The hydrophilic photonic crystal gel was constructed with a $SiO_2$ colloidal crystal array, and poly(ethylene glycol) methacrylate and ethylene glycol were used as the sensing materials (Fig. 5b). The adequately tested solvents resulted in a database of dynamic reflection spectral patterns, which provide a standard for identifying unknown solvents.

Due to the porous properties of the inverse opal structure, the inverse opal structural color is more easily adjusted by changing the RI of the medium phase than the opal structural color.[91] Qian *et al.*[92] utilized the aggregation of biomolecules in the inverse opal colloidal crystal film for the identification of immunoreaction and formulated a quantitative analysis of the target molecule. In addition, a high RI contrast between the building blocks and medium phase can be achieved by assembling hollow colloidal particles. Clays *et al.*[93] assembled monodisperse $SiO_2$ hollow particles into PCSs to introduce optically invisible patterns. As the dense $SiO_2$ shell prevents liquids from penetrating into the core, which creates large RI contrast with the air inside the spheres, PCS results in not only a significant PBG shift (structural color change) of ≈63 nm in the patterned regions, but also better visibility to the naked eye, which is difficult to achieve in traditional PCSs comprising solid spheres (Fig. 5c).

### 5.2 Modulation of crystal lattices

The change in the lattice constant, also called the space between the particles in 3D PCSs, is the most widely used modulation approach for structural color. Lòpez *et al.*[94] found that the optical properties of packed monodisperse $SiO_2$ particles can be easily tuned through their particle size. In addition, the lattice constant can also be modulated by adjusting the wettability of hydrogels. Gu *et al.*[95] realized label-free visual detection by a change in the crystal lattice (Fig. 6a). They combined aptamer, a new molecular recognition unit, to fabricate an aptamer-based PCS intelligent hydrogel sensor. The lattice and structural color changed when the binding aptamer connected the target metal ions. Based on such PCS gel, the analysis for different target materials can be achieved by changing the aptamers chain immobilized on the colloidal crystals gel, which promotes the development of visual detection technology.

The lattice of the structural color materials with a non-close-packed structure tends to be tuned by mechanical deformation.

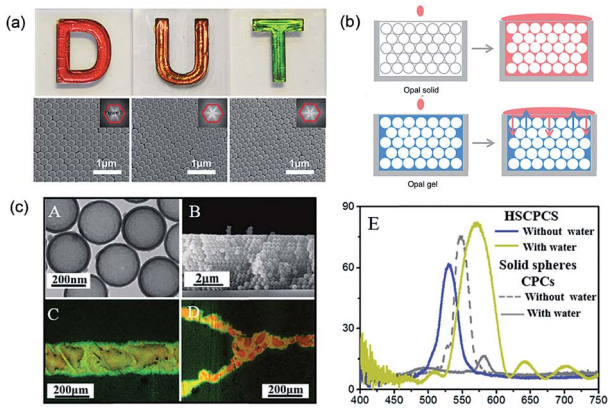


Fig. 5 (a) Digital photographs and SEM images (insets: corresponding FFT images) of structural color films on a white background self-assembled by polysulfide colloidal particles having different particle sizes (D: 260 nm; U: 244 nm; T: 211 nm). Reproduced with permission.[88] Copyright 2016, John Wiley and Sons. (b) "Static reflection spectrum" (top) and "dynamic reflection spectrum" (bottom) detection based on the red-shift of balanced reflection wavelength. Reproduced with permission.[90] (c) (A) TEM image of hollow $SiO_2$ particles. (B) SEM image of the cross-section of hollow $SiO_2$ PCSs. (C and D) The introduced line shape and Y-junction channels in hollow $SiO_2$ PCSs with water for visualization of the superhydrophilic channels. (E) Reflectance spectra of hollow $SiO_2$ PCSs taken from the etched regions with and without water infiltration when compared with the same effect in conventional PCSs. Reproduced with permission.[93] Copyright, 2016, Royal Society of Chemistry.

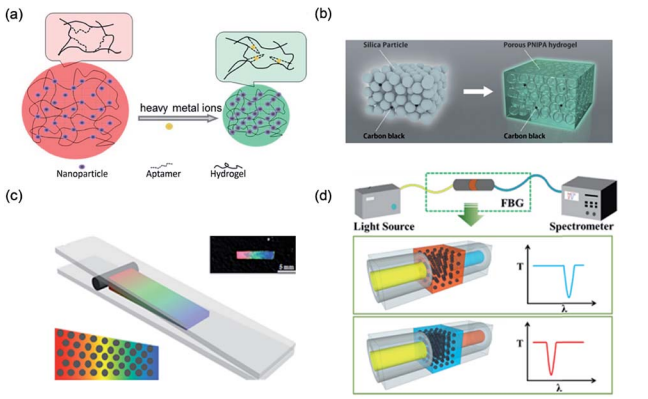


Fig. 6 (a) Schematic depiction of a structurally colored hydrogel aptasensor for the detection of heavy metal ions. Reproduced with permission.[95] Copyright 2012, Royal Society of Chemistry. (b) Preparation of a structurally colored porous thermosensitive hydrogel using a colloidal amorphous array. Reproduced with permission.[103] Copyright 2015, Wiley-VCH. (c) Schematic illustration of the fabrication of a spectrometer grating and the optical image of the obtained grating film with a black pane. Reproduced with permission.[100] Copyright 2014, American Chemical Society. (d) Schematic diagram of the system structure and principle of the structural color filter with a regulated filter band. Reproduced with permission.[101] Copyright 2013, Royal Society of Chemistry. (d) Preparation of a structurally colored porous thermosensitive hydrogel using a colloidal amorphous array. Reproduced with permission.[103] Copyright 2015, Wiley-VCH.

Pressure regulation is a direct and effective way to regulate the lattice distance of the non-close-packed colloidal PCSs. When the structural color materials are subjected to external pressures, the spacing of the lattice is compressed, and therefore, reduces; this changes the color.[96–99] Based on the pressure regulation in the field of colloidal particle self-assembly, Gu *et al.* designed a structural color diffraction grating that covered the visible light band.[100] Because of the excellent pressure response of the hydrogel network, the structural color of the film blue-shifted under pressure (Fig. 6b). Gu *et al.* also developed an optical fiber dynamic filter to fabricate a Bragg reflector by connecting the modulated non-close-packed colloidal PCS hydrogel membranes with the two ends of the optical fiber.[101] The dynamic regulation of the Bragg grating wavelength could be achieved by adjusting the thickness of the film, and the Bragg grating wavelength decreased linearly with an increase in the compression degree of the film. In addition, the addition of multiple grating films in the same fiber channel could yield the joint regulation of the optical signals in a larger wavelength range (Fig. 6c).

Apart from opal PCSs, the structural color with inverse opal PCSs could also be adjusted by the crystal lattice. Omenetto *et al.*[102] reported the modulation of the structural color of a silk inverse opal using 3D lattice conformational control. The photonic lattice and structural definition can be controllably altered by water vapor and UV light exposure. The precise spectral response and spatial controllability, combined with the versatility of silk, endow the structural color of large-scale silk inverse opal with promising new avenues for photonic applications. Similar to PCSs, structural color materials involving PASs could also change colors attributable to wavelength-specific constructive interference in the visible region in response to external stimuli. For this, Takeoka *et al.*[103] reported porous poly(*N*-isopropylacrylamide) hydrogels prepared by colloidal amorphous array templates. The obtained PAS hydrogels with angle-independent structural colors exhibited rapid changes in the volume in response to temperature variations. This facile method may be widely applicable to many other structural color-based stimuli-sensitive soft materials (Fig. 6d).

# 6. Applications of structurally colored materials of colloidal arrays

## 6.1 Structurally colored contact lenses

Structural color is an optimal candidate for use as a coloring method for contact lenses because it has vivid iridescence and is free of pigments. In the structure of the human eye, the area in the iris generates color only due to a micro-ordered structure. The natural structural color inspired researchers to create ordered structures in the lenses and produce structural colored contact lenses. Lowe *et al.*[104] first used the holographic laser technology to fabricate a colored contact lens with an ordered microstructure. However, this fabrication method requires expensive precision optical equipment, and most importantly, the high risk from residual silver nanoparticles embedded in the lens remains an enormous challenge. To address this, Gu *et al.*[105] explored a novel structural color paint to produce a contact lens with structural color by UV polymerization in a mold (Fig. 7a). The paints were fabricated by dispersing poly(methyl methacrylate)–hydroxyethyl methacrylate nanoparticles in a 2-hydroxyethyl methacrylate solvent to form a non-close-packed structural color paint without additional surfactants. The obtained contact lens with structural color presented high light transmission, spectacular structural color, and cytocompatibility. Although the structural color hydrogels with non-close-packed design are proper biomaterials for contact lenses, the design of a color overlay for the entire lens had a strong impact on the light transmission in the pupil area during wearing. Therefore, Gu's group[106] also reported a coffee-ring circular structural colored contact lenses to resolve this problem. The strategy for fabricating such a kind of lens was replicating a circular colloidal PCS template, which was one-step self-assembled into molds based on the coffee-ring effect. The prepared contact lenses exhibited brilliant colors (Fig. 7b). Structural colored contact lenses have many additional functions because of their unique structure; for example, Lai *et al.*[107] fabricated a novel contact lens with antireflective properties for UV and blue light. The proposed contact lenses not only blocked UV and blue light under sunlight, but also avoided the risk of harm posed by chemical dyes present in commercial colored contact lenses.

When compared with the traditional structures, structural colored contact lenses have the following advantages: (1) the physical color mechanism of structural color is harmless to the eye; (2) the production process of structural colored contact lenses is simpler and easier; and (3) the color of the lens is brighter and more stable than that produced by chemical dyes because it is generated by a physical method. In addition, based on the lattice modulation of structural color materials, by coupling with an environmentally sensitive hydrogel, this kind of contact lens could be used as a sensing lens for pH and glucose monitoring.

## 6.2 Optical microfluidic chip

In the recent years, microfluidic chip technology has rapidly developed in the field of chemical–biological sensing. Song *et al.*[108] introduced PCSs into a microchip by constructing

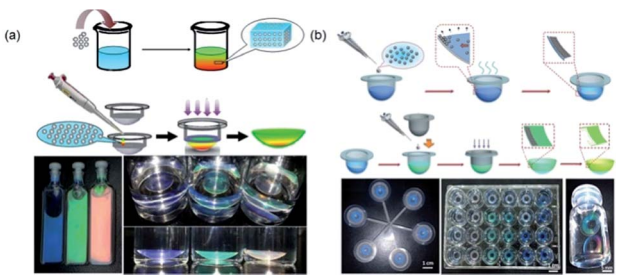


Fig. 7 (a) Schematic depiction of structural colored contact lens with color overlaid on the entire lens and the obtained three colored paint and lenses. Reproduced with permission.[105] Copyright 2016, Royal Society of Chemistry. (b) Schematic depiction of coffee-ring circular structural colored contact lenses, circular colloidal crystal template, and the obtained different colored paints. Reproduced with permission.[106] Copyright 2014, Wiley-VCH.

a hydrophilic PCS microfluidic channel on a hydrophobic substrate through inkjet printing. The hydrophilic or hydrophobic PCS-patterned microchip guided the solution in spreading along the channel and did not wet the hydrophobic region because of the capillarity of PCSs and the wettability difference between the hydrophilic channel and hydrophobic region. Based on the ordered porous and fluorescence enhancement effect of PCSs, the structural color materials in the microfluidic chip achieved the functionalization and integration of the micro- or nanodetection device.[109–111] Gu *et al.* reported a pseudo-paper microfluidic chip based on patterned photonic nitrocellulose, *i.e.*, PCS channels were fabricated by sacrificing opal $SiO_2$ nanoparticle templates (Fig. 8a).[112] Because of its capillarity and hydrophilicity, the flow profile of the aqueous solution wicking through the channel was more uniform than that for a conventional paper-based microfluidic chip. The wicking rate of the aqueous solution through the hollow channel could be easily controlled by altering the size of the nanoparticles, which determined the pore size of the PCS channel. The PBG of PCSs could also be controlled by the propagation of light, enhancing spontaneous radiation and providing a new way to improve the sensitivity of fluorescence detection. In addition to the porous property, Gu *et al.* used the fluorescence enhancement effects of structural color for the detection of adenosine triphosphate and thrombin for the fabrication of analytical capillary devices for point-of-care testing (Fig. 8b).[113] Owing to the fluorescence enhancement effect of the photonic heterostructures, the fluorescence signal for detection was amplified by a factor of up to 40. In addition, Gu *et al.* also applied the fluorescence enhancement effect of structural color in a wearable monitoring sensor for multiplex detection of two proteins (*i.e.*, IgG and AD7c-NTP) and achieved highly sensitive detection, which facilitated the diagnosis of neurodegenerative diseases.[114] The wearable sensor was designed by combining a flexible electronic sensor and microfluidic analytical device and placed on *Morpho menelaus*. Further study revealed that the wearable biosensor could enable the biochemical–physiological hybrid monitoring of neurodegenerative diseases (Fig. 8c). By integrating the photonic colloidal crystal in the paper channels, Gu *et al.* developed a fish-like biosensor to realize sweat collection, diagnostics, and fluorescence enhancement detection for sweat lactic acid and urea.[115] The resistance could sensitively change as the stretchable electronic paper network moved (Fig. 8d).

### 6.3 Structural color displays

The structural color from colloidal assembly has garnered ever-increasing scientific interest for display devices. Unlike dyes or pigments, the bright structural color avoids the problem of chemical or photobleaching, which is widely present in dye/pigment coatings. Ozin *et al.*[116] developed full-color structural color display devices through electrochromic PCSs. The structural color could be altered into red, green, or blue by tuning the voltage applied to the device (Fig. 9a). Gu *et al.*[117] realized a magnetic-field-induced structural color display, which was assembled by magnetic particles. The structural color controllably appeared in different colors by controlling the external magnetic simulation. Nevertheless, the common structural color has a pale, nearly white color display problem when viewed by the naked eye. Some researchers have used black materials to improve the color visibility of structural color by means of doping. For example, Takeoka *et al.*[17,76] doped carbon nanoparticles in $SiO_2$ PASs during the assembly process to improve the color visibility and form a Japanese-style painting

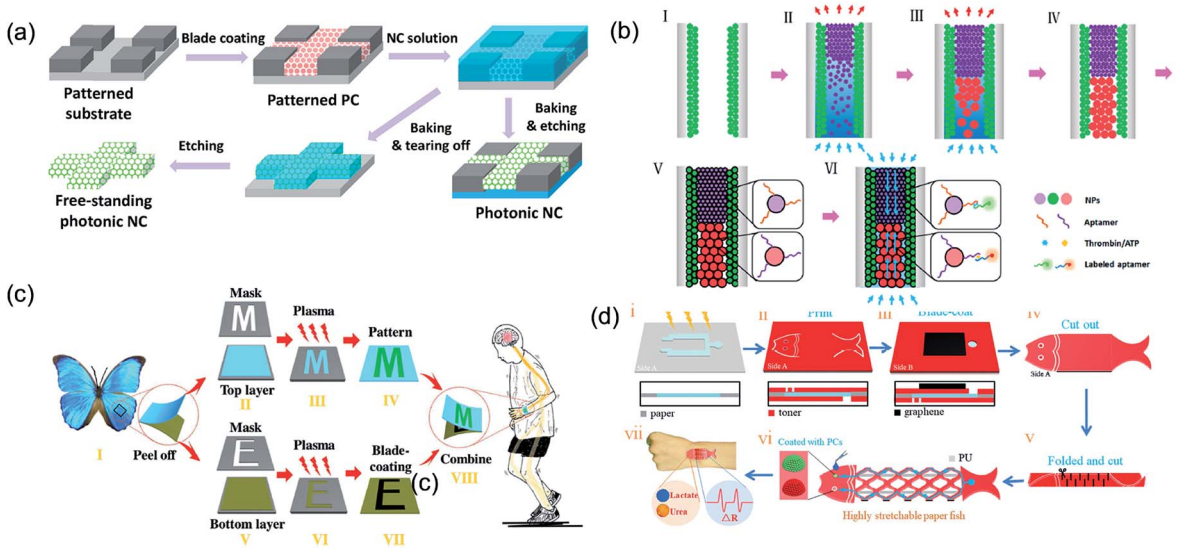


Fig. 8 (a) Schematic illustration showing the procedure for fabricating patterned nitrocellulose PCS channels. Reproduced with permission.[112] Copyright 2016, American Chemical Society. (b) Schematic illustration showing the procedure to fabricate the opal capillary with multiple heterostructures for enhanced fluorescent aptamer-based assays. Reproduced with permission.[113] Copyright 2017, American Chemical Society. (c) Schematic diagram illustrating the fabrication of *M. menelaus*-based wearable sensors. Reproduced with permission.[114] Copyright 2018, Wiley-VCH. (d) Schematic illustration of the paper fish sensor fabrication process. Reproduced with permission.[115] Copyright 2018, Wiley-VCH.

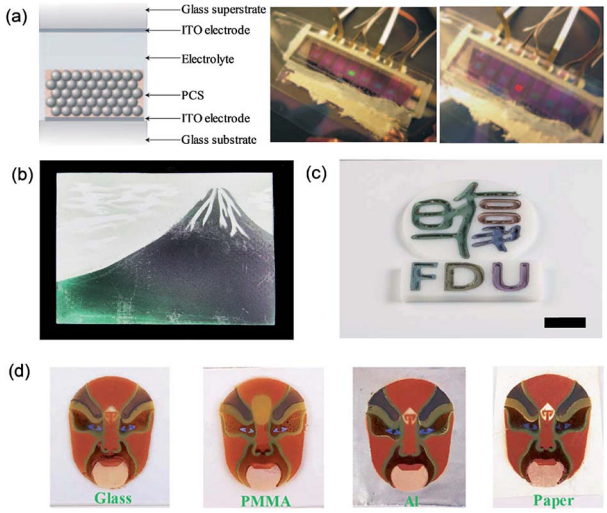


Fig. 9 (a) Full-color PCS display devices based on patterned electromatic PCSs. Reproduced with permission.[116] Copyright 2007, Springer Nature. (b) A color picture of Mount Fuji created by $SiO_2$ PASs and carbon nanoparticles. Reproduced with permission.[17] Copyright 2013, John Wiley and Sons. (c) A colored logo of Fudan University fabricated using six non-iridescent structural colors under oblique observations. Reproduced with permission.[118] Copyright 2015, John Wiley and Sons. (d) Facial makeup patterns induced by PDA@$SiO_2$ PASs coated on various indicated substrates. Reproduced with permission.[74] Copyright 2017, Royal Society of Chemistry.

(Fig. 9b). Zhang *et al.*[118] self-assembled a mixture of monodisperse PS and cuttlefish ink particles to produce mass PASs with a high color visibility based on the drop-coating method. Fig. 9c shows a logo of Fudan University fabricated by highly visible colored arrays. Song *et al.*[119] used graphene nanosheets as an additive to achieve highly saturated and brilliant non-iridescent structural colors. Moreover, to consider the mechanical strength of the visible highly colored structural color material, which is a crucial factor for practical applications, Tang *et al.*[120] introduced carbon nanotubes into the PS photonic crystal structural color films. The obtained films exhibited high color visibility in addition to high mechanical strength. Recently, Gu *et al.* reported the use of self-adhesive building blocks, *i.e.*, PDA-coated $SiO_2$ nanoparticles (PDA@$SiO_2$), to construct strongly colored fast amorphous colloidal arrays.[74] Because of the excellent characteristics of the structural color materials and PDA, the color materials with high fastness and color visibility presented a beautiful facial makeup pattern coated on various substrates (Fig. 9d). Moreover, Wu *et al.*[121] used monodisperse CdS spheres to fabricate large-scale structural color displays on paper by inkjet printing methods. Due to the angle dependence of the structural color, the designed colored patterns could appear clearly and disappear by simply changing the viewing angle.

### 6.4 Structural color sensors

The structural color materials applied in sensors have been developed over the recent decades because of their facile fabrication and largely modified surface. These structural color sensors were usually constructed by responsive materials and could be tuned by corresponding stimuli, such as temperature,[122–124] humidity,[125–127] pH,[128–130] ions,[131–133] and molecules.[134,135] Inspired by *Tmesisternus isabellae*, Gu *et al.*[136] assembled mesoporous $SiO_2$ nanoparticles (MSNs) as assembled colloidal particles. Subsequently, the obtained structural colored patterns possessed a strong response to vapor because of the change in RI. The vapor-responsive color-shifting properties of the mesoporous structural colored patterns were precisely controlled by the design of MSNs in the printing inks. The responsive structural color pattern with complex implicit images revealed by vapor was composed of three kinds of colored patterns, which displayed the same color in $N_2$, but had different vapor-responsive color-shifting properties in ethanol vapor (Fig. 10a). These complex vapor-responsive color-shifting features of the multicolor pattern were easy to recognize by the naked eye for visual authentication, but it also increases counterfeiters' difficulty in forging copies; therefore, they have promising potential in anticounterfeiting applications. Inspired by nature, Xiao *et al.*[137] first prepared synthetic melanin particles and assembled structural color thin films with a rapid reversible color change in response to a change in the humidity level. With nanoparticles swelling upon water uptake in a humid environment, when the relative humidity increases from 10% to 90%, the thickness of the thin film increases and the reflection peak wavelength shifts from 475 to 530 nm (Fig. 10b). As an improved proposal, Zhong *et al.*[138] introduced

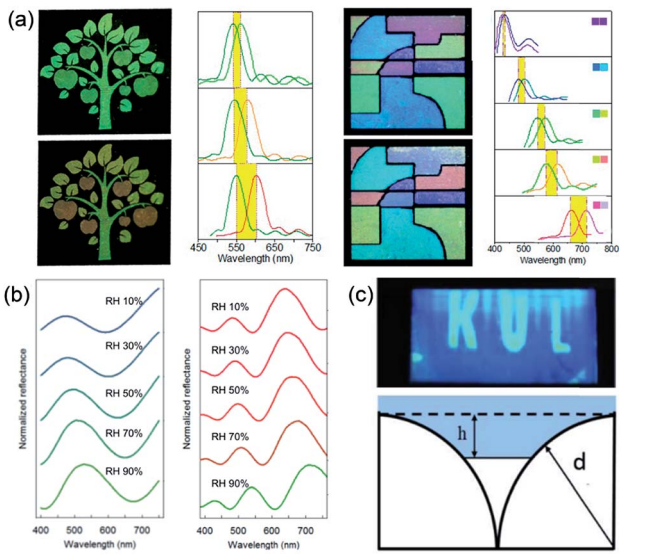


Fig. 10 (a) Color and reflection spectral changes of information hidden in MSN structural colored patterns and multicolor MSN structural colored patterns in $N_2$ and saturated EtOH vapor atmospheres. Each reflection spectrum was marked by colors of the corresponding patterns in the panels. Reproduced with permission.[136] Copyright 2014, American Chemical Society. (b) Reflectance spectra of blue and red films responding to a change in the humidity level. Reproduced with permission.[137] Copyright 2016, American Chemical Society. (c) Optical image after blowing onto it and the model of liquid propagation on the hydrophobic surface of the hollow $SiO_2$ PCSs. Reproduced with permission.[138] Copyright 2018, John Wiley and Sons.

invisible patterns into hollow $SiO_2$ PCSs. The hidden images are formed by creating hydrophilic regions with $O_2$ plasma etching in initially hydrophobic hollow $SiO_2$ PCSs with chemical modification. The invisible patterns show an ultrafast response time ($\approx$100 ms) conveniently revealed by human breath. They also discuss the thermodynamic principles of the revealed hidden patterns, which depend on the surface tension of the vapor, as well as on the high RI contrast (Fig. 10c).

# 7. Outlook

In this review, we have summarized certain recent advances that focus on the generation, modulation, and application of structural color materials using colloidal assembly. Despite these exciting and compelling achievements, a huge gap exists between laboratory research findings and their practical applications because of defective mechanical properties, immature mass-production technology, and limited fields of application. To overcome this, some main issues should be considered for further studies. First, structural color materials that are formed by packing particles have very low mechanical strength, which is a significant barrier in their performance. Therefore, investigating a type of self-adhesive particle, which could cross-link in the particle–particle and particle–substrate manner during the assembly process of the structural color materials may be an effective optional solution. Second, the color gamut is also a very important topic when discussing color. The adjustment of this gamut is one of the key problems of color. Currently, the gamut of most structural colors can only be adjusted by the size of the building blocks, which makes the generated gamut very narrow. Therefore, the development of new structurally colored materials that can generate a wide gamut has always been a difficulty in the study of structural color. Third, large-scale manufacturing and patterning methods for structural color devices need to be developed for real applications. Based on colloidal particle assembly for structural color materials during actual production, an applied assembly technique should be explored with easier operation and higher atomization similar to current processes such as printing and writing. The fourth issue involves the promotion of such applications. It is important to broaden the more valuable properties for the structural color materials and realize their applications in multiple areas, such as clinical, medical, food, and environmental fields. In view of their nontoxic and eco-friendly merits, structural color materials based on colloidal particle assembly technologies have bright application prospects.

In addition to the colloidal assembled structural color materials, Mie scattering or surface plasmon effect of metal nanoparticles have also been discussed in structural color materials. Surface plasmon is a collective oscillation pattern formed on a metal surface with free electrons and incident light that produces resonance, displaying specific colors independent of the dye. When the metal surface is small to the nanometer level, localized surface plasmon resonance is formed. For example, gold or silver nanoparticles were used to make colored glass in the church during ancient times. Mie scattering is usually caused by particles alone. Recently, Kim *et al.*[139] successfully fabricated structural colors caused by resonant Mie scattering using melanin-like polydopamine nanoparticles, inspired by human hair. As high absorbance of melanin suppresses multiple scattering, various colors can be fabricated according to the particle size.

Summarily, structural color materials are modulated by the light propagation characteristics of the interaction between light and matter. With continuous progress on micro/nanoscale manufacturing technologies and materials science, researchers will have more abundant approaches to study and use colloidal particles, generating a variety of high-performance structural color materials that can find prevalence in information, energy, health, environmental resources, and other fields.

## Conflicts of interest

The authors declare no conflict of interest.

## Acknowledgements

This work was supported by the Research Fund of the National Key Research and Development Program of China (No. 2017YFA0205700), National Natural Science Foundation (No. 21872026, 21635001, 21327902), the "111" Project of Ministry of Education of China (No. B17011), the Natural Science Foundation of Jiangsu Province (Grant BK20150024), the Key Research and Development Plan of Jiangsu Province BE2016002, the Project of Special Funds of Jiangsu Province for the Transformation of Scientific and Technological Achievements (Grant No. BA2015067), and the Fundamental Research Funds for the Central Universities (2632017PY02).

## Notes and references

1 S. Kinoshita, S. Yoshioka, Y. Fujii and N. Okamoto, *Forma*, 2002, **17**, 103.
2 H. M. Whitney, M. Kolle, P. Andrew, L. Chittka, U. Steiner and B. J. Glover, *Science*, 2009, **323**, 130.
3 X. F. Gao, X. Yan, X. Yao, L. Xu, K. Zhang, J. Zhang, B. Yang and L. Jiang, *Adv. Mater.*, 2007, **19**, 2213.
4 H. Yin, B. Dong, X. Liu, T. Zhan, L. Shi, J. Zi and E. Yablonovitch, *Proc. Natl. Acad. Sci. U. S. A.*, 2012, **109**, 10798.
5 B. Q. Dong, X. H. Liu, T. R. Zhan, L. P. Jiang, H. W. Yin, F. Liu and J. Zi, *Opt. Express*, 2010, **18**, 14430.
6 A. R. Parker, V. L. Welch, D. Driver and N. Martini, *Nature*, 2003, **426**, 786.
7 P. Vukusic, *Phys. World*, 2004, **17**, 35.
8 A. R. Parker, *Proc. R. Soc. London, Ser. B*, 1998, **265**, 967.
9 T. F. Anderson and A. Glenn Richards, *J. Appl. Phys.*, 1942, **13**, 748.
10 A. R. Parker, R. C. McPhedran, D. R. McKenzie, L. C. Botten and N.-A. P. Nicorovici, *Nature*, 2001, **409**, 36.
11 A. R. Parker, *J. Opt. A: Pure Appl. Opt.*, 2000, **2**, R15.
12 E. Yablonovitch, *Phys. Rev. Lett.*, 1987, **58**, 2059.
13 S. John, *Phys. Rev. Lett.*, 1987, **58**, 2486.

 

14 J. M. Weissman, H. B. Sunkara, A. S. Tse and S. A. Asher, *Science*, 1996, **274**, 959.
15 S. A. Asher, J. Holtz, L. Liu and Z. Wu, *J. Am. Chem. Soc.*, 1994, **116**, 4997.
16 O. L. Pursiainen, J. J. Baumberg, H. Winkler, B. Viel, P. Spahn and T. Ruhl, *Opt. Express*, 2007, **15**, 9553.
17 Y. Takeoka, S. Yoshioka, A. Takano, S. Arai, K. Nueangnoraj, H. Nishihara, M. Teshima, Y. Ohtsuka and T. Seki, *Angew. Chem., Int. Ed.*, 2013, **52**, 7261.
18 M. Harun-Ur-Rashid, A. B. Imran, T. Seki, M. Ishi, H. Nakamura and Y. Takeoka, *ChemPhysChem*, 2010, **11**, 579.
19 R. O. Prum, R. H. Torres, S. Williamson and J. Dyck, *Nature*, 1998, **396**, 28.
20 L. Shi, Y. Zhang, B. Dong, T. Zhan, X. Liu and J. Zi, *Adv. Mater.*, 2013, **25**, 5314.
21 E. R. Dufresne, H. Noh, V. Saranathan, S. G. J. Mochrie, H. Cao and R. O. Prum, *Soft Matter*, 2009, **5**, 1792.
22 H. Noh, S. F. Liew, V. Saranathan, S. G. J. Mochrie, R. O. Prum, E. R. Dufresne and H. Cao, *Adv. Mater.*, 2010, **22**, 2871.
23 B. Q. Dong, X. H. Liu, T. R. Zhan, L. P. Jiang, H. W. Yin, F. Liu and J. Zi, *Opt. Express*, 2010, **18**, 14430.
24 A. I. Kuznetsov, A. E. Miroshnichenko, M. L. Brongersma, Y. S. Kivshar and B. Luk'yanchuk, *Science*, 2016, **354**, 2472.
25 Y. H. Fu, A. I. Kuznetsov, A. E. Miroshnichenko, Y. F. Yu and B. Luk'yanchuk, *Nat. Commun.*, 2013, **4**, 1527.
26 H. Miyazaki, M. Hase, H. T. Miyazaki, Y. Kurokawa and N. Shinya, *Phys. Rev. B: Condens. Matter Mater. Phys.*, 2003, **67**, 235109.
27 Y. Takeoka, *J. Mater. Chem.*, 2012, **22**, 23299.
28 D. Ge, E. Lee, L. Yang, Y. Cho, M. Li, D. S. Gianola and S. Yang, *Adv. Mater.*, 2015, **27**, 2489.
29 I. Lee, D. Kim, J. Kal, H. Baek, D. Kwak, D. Go, E. Kim, C. Kang, J. Chung, Y. Jang, S. Ji, J. Joo and Y. Kang, *Adv. Mater.*, 2010, **22**, 4973.
30 A. C. Arsenault, D. P. Puzzo, I. Manners and G. A. Ozin, *Nat. Photonics*, 2007, **1**, 468.
31 Y. Meng, B. Tang, B. Ju, S. Wu and S. Zhang, *ACS Appl. Mater. Interfaces*, 2017, **9**, 3024.
32 W. Yuan, N. Zhou, L. Shi and K.-Q. Zhang, *ACS Appl. Mater. Interfaces*, 2015, **7**, 14064.
33 V. N. Bogomolov, S. V. Gaponenko, A. M. Kapitonov, A. V. Prokofiev, S. M. Samoilovich, A. N. Ponyavina and N. L. Silvanovich, *The Physics of Semiconductors*, ed. M. Scheffler and R. Zimmermann, 1996, vol. 4, p. 3139.
34 V. N. Bogomolov, S. V. Gaponenko, I. N. Germanenko, A. M. Kapitonov, E. P. Petrov, N. V. Gaponenko, A. V. Prokofiev, A. N. Ponyavina, N. I. Silvanovich and S. M. Samoilovich, *Phys. Rev. E: Stat. Phys., Plasmas, Fluids, Relat. Interdiscip. Top.*, 1997, **55**, 7619.
35 R. Mayoral, J. Requena, J. S. Moya, C. Lòpez, A. Cintas, H. Míguez, F. Meseguer, L. Vázquez, M. Holgado and Á. Blunco, *Adv. Mater.*, 1997, **9**, 257.
36 G. Widawski, M. Rawiso and B. Francois, *Nature*, 1994, **369**, 387.
37 A. R. Parker and Y. Xia, *Adv. Mater.*, 1998, **10**, 1045.
38 A. S. Dimitrov and K. Nagayama, *Langmuir*, 1996, **12**, 1303.
39 P. Jiang, J. F. Bertone, K. S. Hwang and V. L. Colvin, *Chem. Mater.*, 1999, **11**, 2132.
40 S. M. Yang, H. Míguez and G. A. Ozin, *Adv. Funct. Mater.*, 2002, **12**, 425.
41 Y. A. Vlasov, X. Z. Bo, J. C. Sturm and D. J. Norris, *Nature*, 2001, **414**, 289.
42 Z. Gu, A. Fujishima and O. Sato, *Chem. Mater.*, 2002, **14**, 760.
43 L. Woodcock, *Nature*, 1997, **385**, 141.
44 M. Holgado, F. García-Santamaría, A. Blanco, M. Ibisate, A. Cintas, H. Míguez, C. J. Serna, C. Molpeceres, J. Requena, A. Mifsud, F. Meseguer and C. López, *Langmuir*, 1999, **15**, 4701.
45 Z. Gu, Q. Meng, S. Hayami, A. Fujishima and O. Sato, *J. Appl. Phys.*, 2001, **90**, 2042.
46 Q. Meng, Z. Gu and O. Sato, *Appl. Phys. Lett.*, 2000, **77**, 4313.
47 J. Chen, P. Dong, D. Di, C. Wang, H. Wang, J. Wang and X. Wu, *Appl. Surf. Sci.*, 2013, **270**, 6.
48 Z. Gu, D. Wang and H. Möhwald, *Soft Matter*, 2007, **3**, 68.
49 A. V. Blaaderen, R. Ruel and P. Wiltzius, *Nature*, 1997, **385**, 321.
50 P. V. Braun, R. W. Zehner, C. A. White, M. K. Weldon, C. Kloc, S. S. Patel and P. Wiltzius, *Adv. Mater.*, 2001, **13**, 721.
51 S. M. Yang, H. Míguez and G. A. Ozin, *Adv. Funct. Mater.*, 2002, **12**, 425.
52 Z. Gu, A. Fujishima and O. Sato, *Angew. Chem., Int. Ed.*, 2002, **41**, 2067.
53 L. Wu, Z. Dong, M. Kuang, Y. Li, F. Li, L. Jiang and Y. Song, *Adv. Funct. Mater.*, 2015, **25**, 2237.
54 S. H. Kim, S. J. Jeon, G. R. Yi, C. J. Heo, J. H. Choi and S. M. Yang, *Adv. Mater.*, 2008, **20**, 1649.
55 S. H. Kim, S. J. Jeon, W. C. Jeong, H. S. Park and S. M. Yang, *Adv. Mater.*, 2008, **20**, 4129.
56 X. Zhao, Y. Cao, F. Ito, H. H. Chen, K. Nagai, Y. Zhao and Z. Gu, *Angew. Chem., Int. Ed.*, 2006, **45**, 6835.
57 Y. Zhao, X. Zhao, C. Sun, J. Li, R. Zhu and Z. Gu, *Anal. Chem.*, 2008, **80**, 1598.
58 Y. Zhao, X. Zhao, J. Hu, M. Xu, W. Zhao, L. Sun, C. Zhu, H. Xu and Z. Z. Gu, *Adv. Mater.*, 2009, **21**, 569.
59 D. Yang, S. Ye and J. Ge, *J. Am. Chem. Soc.*, 2013, **135**, 18370.
60 C. I. Aguirre, E. Reguera and A. Stein, *Adv. Funct. Mater.*, 2010, **20**, 2565.
61 L. Wang, Q. Yan and X. S. Zhao, *J. Mater. Chem.*, 2006, **16**, 4598.
62 R. Fenollosa and F. Meseguer, *Adv. Mater.*, 2003, **15**, 1282.
63 S. Furumi, T. Kanai and T. Sawada, *Adv. Mater.*, 2011, **23**, 3815.
64 F. Meseguer and R. Fenollosa, *J. Mater. Chem.*, 2005, **15**, 4577.
65 M. Schmudde, C. Grunewald, C. Goroncy, C. N. Noufele, B. Stein, T. Risse and C. Graf, *ACS Nano*, 2016, **10**, 3525.
66 J. J. Bohn, M. Ben-Moshe, A. Tikhonov, D. Qu, D. N. Lamont and S. A. Asher, *J. Colloid Interface Sci.*, 2010, **344**, 298.
67 J. E. Aw, G. T. W. Goh, S. Huang, M. R. Reithofer, A. Z. Thong and J. M. Chin, *Langmuir*, 2015, **31**, 6688.

68 Z. Chen, M. Mo, F. Fu, L. Shang, H. Wang, C. Liu and Y. Zhao, *ACS Appl. Mater. Interfaces*, 2017, **9**, 38901.
69 G. H. Lee, T. M. Choi, B. Kim, S. H. Han, J. M. Lee and S. H. Kim, *ACS Nano*, 2017, **11**, 11350.
70 Y. Takeoka, M. Honda, T. Seki, M. Ishii and H. Nakamura, *ACS Appl. Mater. Interfaces*, 2009, **1**, 982.
71 K. Ueno, A. Inaba, Y. Sano, M. Kondoh and M. Watanabe, *Chem. Commun.*, 2009, **24**, 3603.
72 K. Ueno, Y. Sano, A. Inaba, M. Kondoh and M. Watanabe, *J. Phys. Chem. B*, 2010, **114**, 13095.
73 J. G. Park, S. H. Kim, S. Magkiriadou, T. M. Choi, Y. S. Kim and V. N. Manoharan, *Angew. Chem., Int. Ed.*, 2014, **53**, 2899.
74 P. Liu, J. Chen, Z. Zhang, Z. Xie and Z. Gu, *Nanoscale*, 2018, **10**, 3673.
75 L. Bai, V. C. Mai, Y. Lim, S. Hou, H. Möhwald and H. Duan, *Adv. Mater.*, 2018, 1705667.
76 M. Iwata, M. Teshima, T. Seki, S. Yoshioka and Y. Takeoka, *Adv. Mater.*, 2017, **29**, 1605050.
77 C. F. Lai, Y. C. Wang and H. C. Hsu, *J. Mater. Chem. C*, 2016, **4**, 398.
78 J. D. Forster, H. Noh, S. F. Liew and V. Saranathan, *Adv. Mater.*, 2010, **22**, 2939.
79 Z. Gu, Y. Yu, H. Zhang, H. Chen, Z. Lu, A. Fujishima and O. Sato, *Appl. Phys. A*, 2005, **81**, 47.
80 M. Kuang, J. Wang, B. Bao, F. Li, L. Wang, L. Jiang and Y. Song, *Adv. Opt. Mater.*, 2014, **2**, 34.
81 H. Ding, C. Zhu, L. Tian, C. Liu, G. Fu, L. Shang and Z. Gu, *ACS Appl. Mater. Interfaces*, 2017, **9**, 11933.
82 H. Gu, Y. Zhao, Y. Cheng, Z. Xie, F. Rong, J. Li, B. Wang, D. Fu and Z. Gu, *Small*, 2013, **9**, 2266.
83 X. Su, J. Jiang, X. Sun, S. Wu, B. Tang, W. Niu and S. Zhang, *Nanoscale*, 2017, **9**, 17877.
84 J. Luo, D. Qu, A. Tikhonov, J. Bohn and S. A. Asher, *J. Colloid Interface Sci.*, 2010, **345**, 131.
85 X. Jiang, T. Herricks and Y. Xia, *Adv. Mater.*, 2003, **15**, 1205.
86 A. Kawamura, M. Kohri, G. Morimoto, Y. Nannichi, T. Taniguchi and K. Kishikawa, *Sci. Rep.*, 2016, **6**, 33984.
87 M. Xiao, Y. Li, M. C. Allen, D. D. Deheyn, X. Yue, J. Zhao, N. C. Gianneschi, M. D. Shawkey and A. Dhinojwala, *ACS Nano*, 2015, **9**, 5454.
88 F. Li, B. Tang, S. Wu and S. Zhang, *Small*, 2017, **13**, 1602565.
89 Z. Gu, S. Hayami, Q. Meng, T. Iyoda, A. Fujishima and O. Sato, *J. Am. Chem. Soc.*, 2000, **122**, 10730.
90 Y. Zhang, Q. Fu and J. Ge, *Nat. Commun.*, 2015, **6**, 7510.
91 J. E. G. J. Wijnhoven and W. L. Vos, *Science*, 1998, **281**, 802.
92 W. Qian, Z. Gu, A. Fujishima and O. Sato, *Langmuir*, 2002, **18**, 4526.
93 K. Zhong, M. Khorshid, J. Q. Li, K. Markey, P. H. Wagner, K. Song, S. Van Cleuvenbergen and K. Clays, *J. Mater. Chem. C*, 2016, **4**, 7853.
94 H. Miguez, C. Lòpez, F. Meseguer, A. Blanco, L. Vazquez, R. Mayoral, M. Ocana, V. Fornes and A. Mifsud, *Appl. Phys. Lett.*, 1997, **71**, 1148.
95 B. Ye, Y. Zhao, Y. Cheng, T. Li, Z. Xie, X. Zhao and Z. Gu, *Nanoscale*, 2012, **4**, 5998.
96 B. Viel, T. Ruhl and G. P. Hellmann, *Chem. Mater.*, 2007, **19**, 5673.
97 O. L. J. Pursiainen, J. J. Baumberg, H. Winkler, B. Viel, P. Spahn and T. Ruhl, *Adv. Mater.*, 2008, **20**, 1484.
98 Y. F. Yue, M. A. Haque, T. Kurokawa, T. Nakajima and J. P. Gong, *Adv. Mater.*, 2013, **25**, 3106.
99 F. Castles, S. M. Morris, J. M. C. Hung, M. M. Qasim, A. D. Wright, S. Nosheen, S. S. Choi, B. I. Outram, S. J. Elston, C. Burgess, L. Hill, T. D. Wilkinson and H. J. Coles, *Nat. Mater.*, 2014, **13**, 817.
100 H. Ding, C. Liu, H. Gu, Y. Zhao, B. Wang and Z. Gu, *ACS Photonics*, 2014, **1**, 121.
101 H. Ding, Y. Cheng, H. Gu, Y. Zhao, B. Wang and Z. Gu, *Nanoscale*, 2013, **5**, 11572.
102 Y. Wang, D. Aurelio, W. Li, P. Tseng, Z. Zheng, M. Li, D. L. Kaplan, M. Liscidini and F. G. Omenetto, *Adv. Mater.*, 2017, **29**, 1702769.
103 Y. Ohtsuka, T. Seki and Y. Takeoka, *Angew. Chem., Int. Ed.*, 2015, **54**, 15368.
104 A. Domschke, W. March, S. Kabilan and C. Lowe, *Diabetes Technol. Ther.*, 2006, **8**, 89.
105 P. Liu, Z. Xie, F. Zheng, Y. Zhao and Z. Gu, *J. Mater. Chem. B*, 2016, **4**, 5222.
106 Z. Xie, L. Li, P. Liu, F. Zheng, L. Guo, Y. Zhao and Z. Gu, *Small*, 2015, **11**, 926.
107 C.-F. Lai, J.-S. Li, Y.-T. Fang, C.-J. Chien and C.-H. Lee, *RSC Adv.*, 2018, **8**, 4006.
108 W. Shen, M. Li, C. Ye, L. Jiang and Y. Song, *Lab Chip*, 2012, **12**, 3089.
109 H. Li, J. Wang, F. Liu, Y. Song and R. Wang, *J. Colloid Interface Sci.*, 2011, **356**, 63.
110 J. Hou, H. Zhang, Q. Yang, M. Li, Y. Song and L. Jiang, *Angew. Chem., Int. Ed.*, 2014, **53**, 1.
111 H. Ning, A. Mihi, J. B. Geddes III, M. Miyake and P. V. Braun, *Adv. Mater.*, 2012, **24**, 153.
112 B. Gao, H. Liu and Z. Gu, *Anal. Chem.*, 2016, **88**, 5424.
113 B. Gao, L. Tang, D. Zhang, Z. Xie, E. Su, H. Liu and Z. Gu, *ACS Appl. Mater. Interfaces*, 2017, **9**, 32577.
114 Z. He, A. Elbaz, B. Gao, J. Zhang, E. Su and Z. Gu, *Adv. Healthcare Mater.*, 2018, 1701306.
115 B. Gao, A. Elbaz, Z. He, Z. Xie, H. Xu, S. Liu, E. Su, H. Liu and Z. Gu, *Adv. Mater. Technol.*, 2018, 1700308.
116 A. C. Arsenault, D. P. Puzzo, I. Manners and G. A. Ozin, *Nat. Photonics*, 2007, **1**, 468.
117 C. Zhu, W. Xu, L. Chen, W. Zhang, H. Xu and Z.-Z. Gu, *Adv. Funct. Mater.*, 2011, **21**, 2043.
118 Y. Zhang, B. Dong, A. Chen, X. Liu, L. Shi and J. Zi, *Adv. Mater.*, 2015, **27**, 4719.
119 Y. Zhang, P. Han, H. Zhou, N. Wu, Y. Wei, X. Yao, J. Zhou and Y. Song, *Adv. Funct. Mater.*, 2018, **28**, 1802585.
120 F. Li, B. Tang, J. Xiu and S. Zhang, *Molecules*, 2016, **21**, 547.
121 S. Wu, B. Liu, X. Su and S. Zhang, *J. Phys. Chem. Lett.*, 2017, **8**, 2835.
122 H. Kye, Y. G. Koh, Y. Kim, S. G. Han, H. Lee and W. Lee, *Sensors*, 2017, **17**, 1398.
123 Y. Gotoh, H. Suzuki, N. Kumano, T. Seki, K. Katagiri and Y. Takeoka, *New J. Chem.*, 2012, **36**, 2171.

 

124 H. Sugiyama, T. Sawada, H. Yano and T. Kanai, *J. Mater. Chem. C*, 2013, **1**, 6103.
125 H. Wang, S. Yang, S.-N. Yin, L. Chen and S. Chen, *ACS Appl. Mater. Interfaces*, 2015, **7**, 8827.
126 S. Shang, Q. Zhang, H. Wang and Y. Li, *J. Colloid Interface Sci.*, 2017, **485**, 18.
127 M. M. Hawkeye and M. J. Brett, *Adv. Funct. Mater.*, 2011, **21**, 3652.
128 M. Chen, L. Zhou, Y. Guan and Y. Zhang, *Angew. Chem., Int. Ed.*, 2013, **52**, 9961.
129 J.-G. Park, W. B. Rogers, S. Magkiriadou, T. Kodger, S.-H. Kim, Y.-S. Kim and V. N. Manoharan, *Opt. Mater. Express*, 2017, **7**, 253.
130 A. K. Yetisen, H. Butt and S.-H. Yun, *ACS Sens.*, 2016, **1**, 493.
131 J. Cui, W. Zhu, N. Gao, J. Li, H. Yang, Y. Jiang, P. Seidel, B. J. Ravoo and G. Li, *Angew. Chem., Int. Ed.*, 2014, **53**, 3844.
132 X. Li, L. Peng, J. Cui, W. Li, C. Lin, D. Xu, T. Tian, G. Zhang, D. Zhang and G. Li, *Small*, 2012, **8**, 612.
133 T. Chen, Z.-Y. Deng, S.-N. Yin, S. Chen and C. Xu, *J. Mater. Chem. C*, 2016, **4**, 1398.
134 F. Xue, Z. H. Meng, F. Y. Wang, Q. H. Wang, M. Xue and Z. B. Xu, *J. Mater. Chem. A*, 2014, **2**, 9559.
135 X. Hong, Y. Peng, J. Bai, B. Ning, Y. Liu, Z. Zhou and Z. Gao, *Small*, 2014, **10**, 1308.
136 L. Bai, Z. Xie, W. Wang, C. Yuan, Y. Zhao, Z. Mu, Q. Zhong and Z. Gu, *ACS Nano*, 2014, **8**, 11094.
137 M. Xiao, Y. Li, J. Zhao, Z. Wang, M. Gao, N. C. Gianneschi, A. Dhinojwala and M. D. Shawkey, *Chem. Mater.*, 2016, **15**, 5516.
138 K. Zhong, J. Li, L. Liu, S. V. Cleuvenbergen, K. Song and K. Clays, *Adv. Mater.*, 2018, **30**, 1707246.
139 S. Cho, T. S. Shim, J. H. Kim, D.-H. Kim and S.-H. Kim, *Adv. Mater.*, 2017, **29**, 1700256.